LETTERS

Controlled Sliding and Pullout of Nested Shells in Individual Multiwalled Carbon Nanotubes

Min-Feng Yu,[†] Boris I. Yakobson,[‡] and Rodney S. Ruoff*[,†]

Physics Department, Washington University in St. Louis, St. Louis, Missouri 63130, and Mechanical Engineering & Materials Science Department and Center for Nanoscale Science and Technology, Rice University, Houston, Texas 77005

Received: August 4, 2000

A mechanical-loading stage operating inside a scanning electron microscopy (SEM) was used to realize the sliding between nested shells of multiwalled carbon nanotubes (MWCNTs). A stick−slip motion and a smooth pullout motion were observed for the two separate MWCNTs studied. A model that includes the shear interaction, the "capillary" effect, and the edge effect, was used to explain the observed sliding between nested shells. The shear strength between shells was determined and the surface energy of the MWCNT shell estimated.

Carbon nanotubes, including both multiwalled carbon nanotubes (MWCNTs) and single-walled carbon nanotubes (SWCNTs), are fascinating low dimensional systems for studies in electronics and mechanics. Their applications in nano-electronic or nano-mechanical systems have been suggested. For example, on-nanotube devices such as diode, bucky shuttle, or multiple terminal logic circuits have been treated by theory for electronic systems,[1−4] and the use of nanotubes as nano-pistons, nano-syringes, and rotors for mechanical systems has also been modeled.[5−7]

Experiment has shown that carbon nanotubes can be metallic or semiconducting one-dimensional wires and their quantum characteristics[8−10] have been explored. In contrast, there has been less experimental study of their mechanical and nanotribological properties,[11,12] which is of interest because of the low dimensionality and the expected perfect or near-perfect crystalline structure of nanotubes. To use nanotubes in nano-mechanical systems, achieving an understanding of their nanotribological properties is very important. For example, how will nanotubes interact with each other, or with other surfaces, when in motion?

How either commensurate, or highly incommensurate, crystalline surfaces in motion interact is currently a topic of great interest in nanotribology research.[13−15] Such sliding experiments between surfaces are difficult. Here, we exploit the inherent structure of MWCNTs to perform experiments on the sliding of structurally perfect or near-perfect nested shells. MWCNTs consist of coaxial cylindrical shells of rolled graphene sheets. The spacing between neighboring shells is ∼0.34 nm, similar to the interlayer spacing in graphite. These shells thus interact with each other via van der Waals forces.

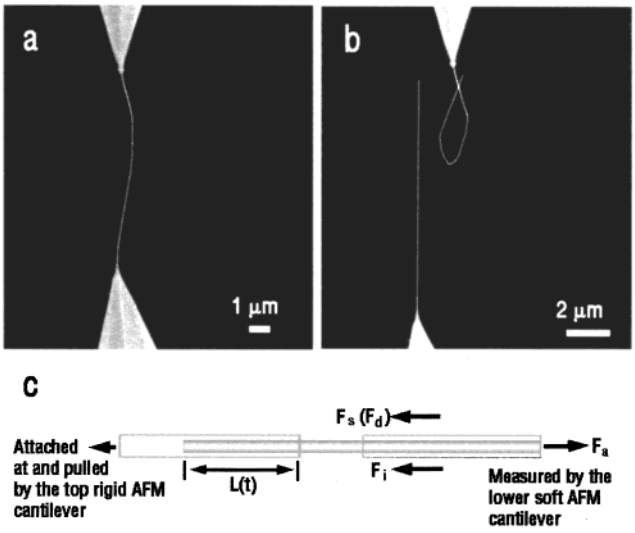

Figure 1. SEM images showing the sword-in-sheath breaking mechanism of MWCNTs. (a) A MWCNT attached between AFM tips under no tensile load. (b) The same MWCNT after being tensile loaded to break. Notice the apparent overall length change of the MWCNT fragments after break compared to the initial length and the curling of the top MWCNT fragment in (b). (c) A schematic showing the sliding and pulling out of internal shells from the outer shell of the MWCNT. The contact length $L(t)$, and the force diagram for the outermost shell (for the model used) are described in the text.

We previously reported tensile-loading experiments on individual MWCNTs using a nano-stressing stage onto which AFM tips are mounted to apply load and as force sensors. The MWCNTs were found to fracture by a sword-in-sheath mechanism.[16] Detailed information about the nano-stressing stage and the experimental procedure can be found elsewhere.[16,17] Figure 1 illustrates the sword-in-sheath breaking mechanism. Here the summed length of MWCNT fragments after fracture (Figure 1b) is obviously larger than the initial length of the MWCNT

* To whom correspondence should be addressed. E-mail: ruoff@wuphys.wustl.edu. After September 1, 2000: r-ruoff@northwestern.edu.
[†] Washington University in St. Louis.
[‡] Rice University.

10.1021/jp002828d CCC: $19.00
Published on Web 08/24/2000

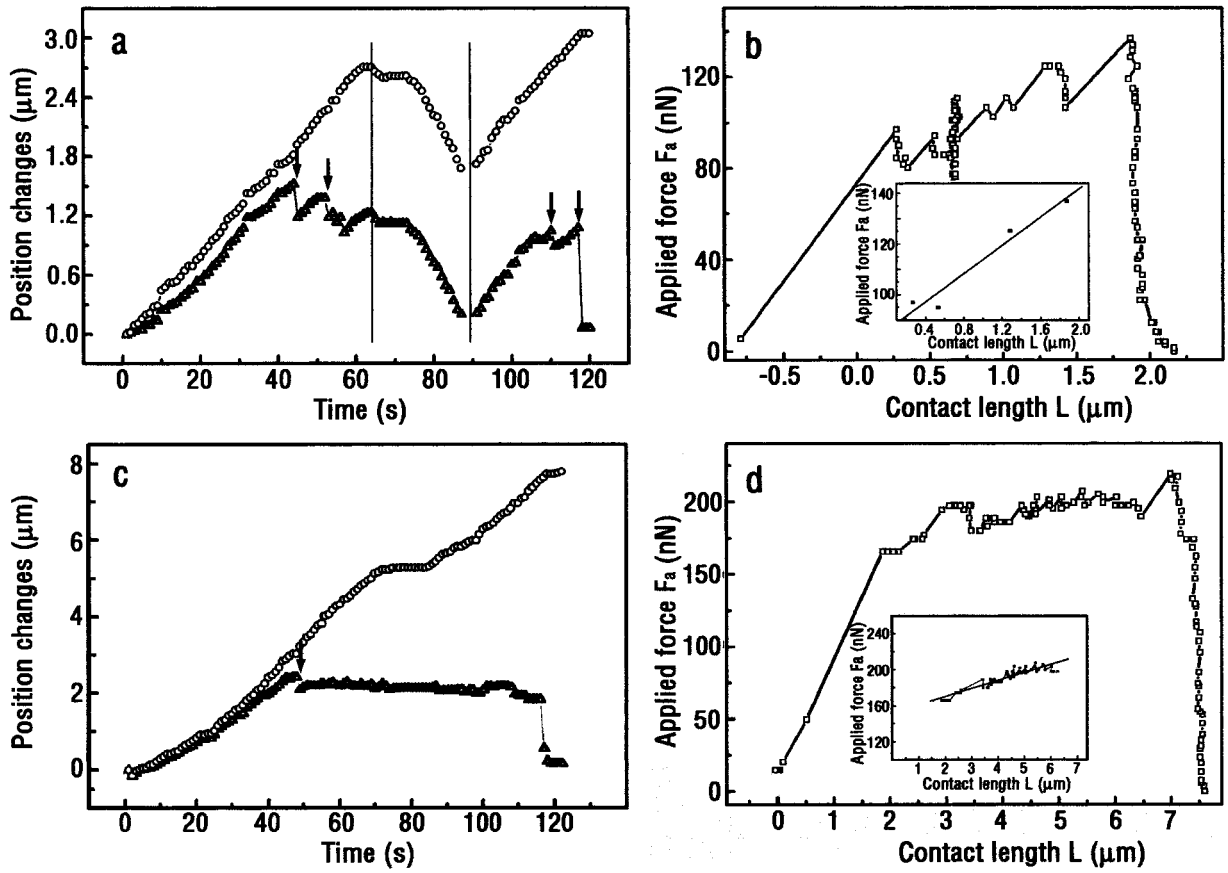

Figure 2. Sliding and pulling out of MWCNT shells. (a) and (c) Time-dependent plots of the positions of the end at the rigid cantilever tip (top curve, open circles) and the end at the soft cantilever tip (lower curve, open triangles) of MWCNT1 (a) and MWCNT2 (c). (b) and (d) F_a vs $L(t)$ plots for MWCNT1 (b) and MWCNT2 (d). Inset in (b): linear fit to F_a at "stick" events (marked by arrows in (a)) as a function of L(t) for MWCNT1. Inset in (d): linear fit to the applied force for MWCNT2 as a function of the contact length for the smooth pullout portion in (d).

before fracture (Figure 1a). After the internal shells have been pulled away from the top fragment in Figure 1b, the fragment evidently became very flexible and curled.

Thus, one method of creating an experimental configuration for measuring the forces involved in the relative motion of nested cylinders in a MWCNT is to first tensile load the outermost shell until it breaks. Figure 1c illustrates the experiment. When pulling apart the fractured MWCNT sections, the force due to outer shell/inner shell interaction can be measured by recording the deflection of the soft cantilever as a function of time. The full experiment is recorded on video. Time-dependent force and distance data are then collected after digitizing the recorded video.

Typically, the large snap back of the soft cantilever just after the MWCNT breaks causes the total separation of the fragments, so the sliding measurement cannot be done. Out of 16 tensile-loading experiments, there were two cases where the fragments did not separate following fracture, largely due to the break happening under a small tensile load. These two MWCNTs, referred to as MWCNT1 and MWCNT2 below, were used to study the sliding mechanism of the outer shell with respect to the inner shells.

Figure 2a shows a plot of the change of the position at each of the MWCNT1 ends versus time. Two curves are shown in the plot. The top curve shows the position change of the MWCNT end attached to the rigid AFM tip, relative to its initial position at $t = 0$. (This position change tracked the manually controlled motion of the piezo-drive to which the rigid AFM probe was attached.) The lower curve shows the position change of the end attached to the soft AFM tip, relative to its initial relaxed position at $t = 0$; this position change also corresponds to the deflection of the soft cantilever. The force applied is calculated as this deflection multiplied by the force constant of the soft cantilever. The soft AFM cantilever has a force constant of 0.09 N/m. (We obtained the force constant of the two different cantilevers used for MWCNT1 and MWCNT2, according to the dimensions of the single crystal Si straight beam cantilever measured by SEM. The force constants were also independently calibrated by AFM, agreeing to within 4% with the calculated values for the two cantilevers used.[18]) Data points in the plot were taken every second from the digitized video.

The rigid AFM tip was manually moved back and forth, as shown in the top curve in Figure 2a. If there is no sliding between the outer shell and the inner shells of MWCNT1, the lower curve should exactly follow the top curve. (The forces applied in this measurement are so low that the change of the internal length of MWCNT shells caused by tension is insignificant because of the inherent stiffness of the nanotube shells in the axial direction.) Once a sliding event occurs between the inner shells and the outer shell, a slip should be visible in the lower curve. Such events are seen in Figure 2a. The contact length $L(t)$ at any time is defined as the length of these overlapped shells that are in sliding contact. That is, $L(t)$ is the length of the "sword" that is still inside the "sheath". The length change $S(t)$ is defined as the difference in position between the top curve and the lower curve at the same time t. The initial contact length h at time $t = 0$ is obtained from the recorded SEM image, thus the contact length $L(t)$ at any time is equal to $h - S(t)$. Figure 2b shows the dependence of the applied force on the contact length obtained from the plot in Figure 2a.

The stick−slip event between shells of MWCNT1 is not due to the shear interaction alone. We model this nano-mechanical system with the following forces as shown in Figure 1c: (i) F_a, the applied force from the deflection of the soft AFM cantilever; (ii) F_s, the static shear interaction force between shells present during the "stick" event; (iii) F_d, the dynamic shear interaction force between shells in the "slip" event; (iv) F_c, the solid−solid "capillary" interface force that is due to the creation of a new shell surface area in the pullout event (surface tension effect); (v) other forces, for example, a force F_e perhaps present and due to the interaction of the dangling bonds on the edge of the fractured MWCNT cylinder with the internal shell surface. We will assume below that F_e, the "edge effect" force, is the main part of the "other forces" that may be present.

The capillary force F_c is defined as $2\pi d\gamma_1$, where d is the diameter of the outer shell of the MWCNT and γ_1 is the surface energy of MWCNT shell. The force F_e is defined as $2\pi d\gamma_2$ because F_e should be proportional to the circumference of the outer shell. An "interface force", $F_i = 2\pi d\gamma$, $\gamma = \gamma_1 + \gamma_2$, is then defined, because we cannot distinguish F_c and F_e. Within this model, when the applied load exceeds the sum of F_i and F_s, sliding occurs between the outer and inner shells. The forces F_i and F_d then counter the applied load F_a, until a force balance is reestablished between the shells in a (new) stable position. The force diagram for the outer shell is shown in Figure 1c. The static shear force F_s between the shells of the MWCNT can be related to the shear interaction strength τ as $F_s = \tau A$, where A is the contact area between shells (equal to $\pi dL(t)$). Thus, $F_a = \pi d\tau L(t) + F_i$.

The inset in Figure 2b shows the plot of F_a vs $L(t)$ obtained for the four "stick" events mark by arrows in the lower curve of Figure 2a. We do not treat some very small slips in the lower curve of Figure 2a or in the plot of Figure 1b and focus on the obvious slips indicated by arrows in the plot. The initial contact length h as obtained from the recorded SEM image is 2.2 μm. The intersection of the linear fit in the inset of Figure 2b to the F axis gives the interface force, $F_i = 85$ nN. The static shear interaction strength value τ determined from the slope $= \pi d\tau$ of the linear fit to the data points in the inset is 0.30 MPa for MWCNT1 ($d = 30$ nm). For comparison, the shear strength value previously reported for that of high quality crystalline graphite ranges from 0.25 to 0.75 MPa (mean value 0.48 MPa).[19]

We show another recorded sliding force measurement on a different MWCNT (MWCNT2) in Figure 2c. The sliding measurement for MWCNT2 is for a longer section (initial contact length of 7.5 μm, outer shell diameter of 36 nm) than for MWCNT1. An obvious feature of Figure 2c is that after the first marked slip the plot reveals the continuous and smooth pullout of the internal shells up until the final sudden pullout, in clear contrast to MWCNT1. The corresponding applied force versus contact length plot is shown in Figure 2d. As stated above, the shear interaction force is proportional to the contact length between the MWCNT2 shells. The observed smooth pullout at an almost constant applied load can be explained if the static shear interaction force is equal to the dynamic shear interaction force. As discussed below, we find that the static and dynamic shear interaction values are both small and indeed equal in magnitude.

The inset in Figure 2d shows the linear fit to the applied force vs contact length curve that is obtained from the flat portion of the lower curve in Figure 2c or Figure 2d. In the fit, the data points corresponding to the interval 70−81 seconds, when the motion of the top cantilever was deliberately stopped, are not included, nor are the data points corresponding to the interval 101−108 seconds, where a plateau is present in the lower curve. (The slope of the plateau is close to the slope of the rest of the curve, which indicates that the pullout mechanism between that time interval is still the same. The small stick−slip event occurring in this interval is not something we explicitly treat here.) We again use the formula $F_a = \pi d\tau L(t) + F_i$ and from the linear fit obtain $F_i = 152$ nN, and $\pi d\tau = 8.8$ nN (μm)$^{-1}$. Thus, the dynamic shear interaction strength is 0.08 MPa. F_a at the "stick" event marked by the arrow in the plot is 219 nN for the 7 μm contact length between shells, which gives a static shear interaction strength of 0.08 MPa. The static and the dynamic shear interaction forces are thus both very small and equal.

The significantly different values of shear interaction strength observed in our measurement can be explained in terms of the anisotropy of friction between the nested shells of different MWCNTs. Since the sliding between the nested shells of a MWCNT can be viewed as similar to the sliding between two atomically flat crystalline surfaces, there is the issue of the degree of commensurability. For a MWCNT, the "degree of commensurability" between two neighboring shells should be dependent on the difference of their helicities. Indeed, a recent theoretical calculation[20] points out that sliding between nested shells of a MWCNT will be anisotropic and the friction will depend on the wrapping angles and the commensurability of the nested shells. The shear strength between nested shells of a MWCNT is found to vary from extremely small to a few MPa.[20] Further experiments may reveal the existence of superlubricity in the sliding between neighboring shells in MWCNTs. The phenomenon of superlubricity occurs when two atomically flat incommensurate surfaces slide relative to each other (thus at a very small friction force).

Another possible explanation for the observation of the different friction in MWCNT1 vs MWCNT2 is that each may have a different interlayer spacing between the neighboring shells. We cannot assess this issue with SEM in the current setup.

We can also obtain the coefficient γ from the interface force F_i as described above. The γ value obtained is 0.45 N m^{-1} (N m^{-1} are identical to J m^{-2}) for MWCNT1 and 0.67 N m^{-1} for MWCNT2. The coefficient γ as defined above has contributions from both the surface energy and the edge effect. The surface energy for graphite was determined to be 0.12 N m^{-1} in 1958.[21] A more recently determined value of the surface energy for graphite, 0.11 N m^{-1}, was obtained from fitting an elastic model for a collapsed carbon nanotube.[22] We define the surface energy as equal to one-half of the cohesion energy, that is, the work needed to separate two unit areas of identical media from contact to infinite separation in a vacuum.[23] Because we cannot separate the contribution from the surface energy from that of the edge effect in our measurement, an exact surface energy value for the MWCNT shell could not be obtained. The values determined for γ for MWCNT1 and MWCNT2 thus provide an upper limit to the surface energy values for each MWCNT studied.

The studies presented here are the first observed and detailed analysis of the sliding of nested shells in multiwalled carbon nanotubes (MWCNTs). The data and analysis presented suggest that theoretical modeling will shed further light on the tribology of sliding nanotube shells. The study should also be useful in providing some design parameters for nano-mechanical engineering systems such as MWCNT pistons, axles, or syringes, where internal cylinders (shells) are repeatedly moved back and forth inside the outer cylinders of the MWCNT.

Acknowledgment. This work is supported by the Office of Naval Research and Defense Advanced Research Programs Agency, the NSF "New Methods and Tools for Nanotechnology", Zyvex, and (for B.I.Y.) the Air Force Research Laboratory. We thank W. Buhro, T. Kowalewski, A. Ruoff, K. Ausman, V. Crespi, and J. Katz for critically reading the manuscript and V. Crespi for sending a preprint (ref 20). We also thank the staff at the NSF-supported Materials Science Center at the University of Wisconsin (UW) for their assistance.

References and Notes

(1) Srivastava, D.; Menon, M. *Mater. Res. Soc. Symp. Proc.* **1998**, *514*, 471.

(2) Kwon, Y.-K.; Tomanek, D.; Iijima, S. *Phys. Rev. Lett.* **1999**, *82*, 1470−1473.

(3) Menon, M.; Srivastava, D. *J. Mater. Res.* **1998**, *13*, 2357−2362.

(4) Treboux, G.; Lapstun, P.; Wu, Z.; Silverbrook, K. *J. Phys. Chem. B* **1999**, *103*, 8671−8674.

(5) Tuzun, R. E.; Noid, D. W.; Sumpter, B. G.; Merkle, R. C. *Nanotechnology* **1996**, *7*, 241−246.

(6) Han, J.; Globus, A.; Jaffe, R.; Deardorff, G. *Nanotechnology* **1997**, *8*, 103−111.

(7) Tuzun, R. E.; Sohlberg, K.; Noid, D. W.; Sumpter, B. G. *Nanotechnology* **1998**, *9*, 37−48.

(8) Hamada, N.; Sawada, S.; Oshiyama, A. *Phys. Rev. Lett.* **1992**, *68*, 1579−81.

(9) Tans, S. J.; Devoret, M. H.; Dal, H.; Thess, A.; Smalley, R. E.; Geerligs, L. J.; Dekker, C. *Nature* **1997**, *386*, 474−477.

(10) Tans, S. J.; Verschueren, A. R. M.; Dekker, C. *Nature* **1998**, *393*, 49−51.

(11) Falvo, M. R.; R. M. T., II; Helser, A.; Chi, V.; F. P. B., Jr.; Washburn, S.; Superfine, R. *Nature* **1999**, *397*, 236−238.

(12) Buldum, A.; Lu, J. P. *Phys. Rev. Lett.* **1999**, *83*, 5050−5053.

(13) Hirano, M.; Shinjo, K.; Kaneko, R.; Murata, Y. *Phys. Rev. Lett.* **1991**, *67*, 2642−2645.

(14) Hirano, M.; Shinjo, K.; Kaneko, R.; Murata, Y. *Phys. Rev. Lett.* **1997**, *78*, 1448−1451.

(15) Muser, M. H.; Robbins, M. O. *Phys. Rev.* **2000**, *61*, 2335−2342.

(16) Yu, M.-F.; Lourie, O.; Dyer, M. J.; Moloni, K.; Kelly, T. F.; Ruoff, R. S. *Science* **2000**, *287*, 637−640.

(17) Yu, M.-F.; Dyer, M. J.; Skidmore, G. D.; Rhors, H. W.; Lu, X. K.; Ausman, K. D.; Ehr, J. R. V.; Ruoff, R. S. *Nanotechnology* **1999**, *10*, 244.

(18) Tortonese, M.; Kirk, M. *Proc. SPIE-Int. Soc. Opt. Eng.* **1997**, *3009*, 53−60.

(19) Soule, D. E.; Nezbeda, C. W. *J. Appl. Phys.* **1968**, *39*, 5122−5139.

(20) Kolmogorov, A. N.; Crespi, V. H. *Phys. Rev. Lett.*, submitted.

(21) Good, R. J.; Girifalco, L. A.; Kraus, G. *J. Chem. Phys.* **1958**, *62*, 1418−1421.

(22) Benedict, L. X.; Chopra, G. N.; Cohen, M. L.; Zettl, A.; Louie, S. G.; Crespi, V. H. *Chem. Phys. Lett.* **1998**, *286*, 490−496.

(23) Israelachvili, J. N. *Intermolecular and surface forces*; Academic Press Inc.: San Diego, 1991.